2014-08-01

Very-High Energy Observations Of The Galactic Center Region By Veritas In 2010-2012

P. T. Reynolds
Cork Institute of Technology

Et. al.

Recommended Citation

Archer, A. et al. (2014) 'VERY-HIGH ENERGY OBSERVATIONS OF THE GALACTIC CENTER REGION BY VERITAS IN 2010-2012', The Astrophysical Journal, 790(2), p. 149. doi: 10.1088/0004-637X/790/2/149.

The Astrophysical Journal, 790:149 (9pp), 2014 August 1 doi:10.1088/0004-637X/790/2/149

VERY-HIGH ENERGY OBSERVATIONS OF THE GALACTIC CENTER REGION BY VERITAS IN 2010–2012

A. Archer[1], A. Barnacka[2], M. Beilicke[1], W. Benbow[3], K. Berger[4], R. Bird[5], J. Biteau[6], J. H. Buckley[1], V. Bugaev[1], K. Byrum[7], J. V Cardenzana[8], M. Cerruti[3], W. Chen[1], X. Chen[9,10], L. Ciupik[11], M. P. Connolly[12], W. Cui[13], H. J. Dickinson[8], J. Dumm[14], J. D. Eisch[8], A. Falcone[15], S. Federici[9,10], Q. Feng[13], J. P. Finley[13], H. Fleischhack[10], L. Fortson[14], A. Furniss[6], N. Galante[3], S. Griffin[16], S. T. Griffiths[17], J. Grube[11], G. Gyuk[11], N. Håkansson[9], D. Hanna[16], J. Holder[4], G. Hughes[10], C. A. Johnson[6], P. Kaaret[17], P. Kar[18], M. Kertzman[19], Y. Khassen[5], D. Kieda[18], H. Krawczynski[1], S. Kumar[4], M. J. Lang[12], G. Maier[10], S. McArthur[20], A. McCann[21], K. Meagher[22], P. Moriarty[12,23], R. Mukherjee[24], D. Nieto[25], A. O'Faoláin de Bhróithe[10], R. A. Ong[26], A. N. Otte[22], N. Park[20], J. S. Perkins[27], M. Pohl[9,10], A. Popkow[26], H. Prokoph[10], E. Pueschel[5], J. Quinn[5], K. Ragan[16], J. Rajotte[16], L. C. Reyes[28], P. T. Reynolds[29], G. T. Richards[22], E. Roache[3], G. H. Sembroski[13], K. Shahinyan[14], A. W. Smith[18], D. Staszak[16], I. Telezhinsky[9,10], J. V. Tucci[13], J. Tyler[16], A. Varlotta[13], S. Vincent[10], S. P. Wakely[20], A. Weinstein[8], R. Welsing[10], A. Wilhelm[9,10], D. A. Williams[6], A. Zajczyk[1], and B. Zitzer[7]

[1] Department of Physics, Washington University, St. Louis, MO 63130, USA; beilicke@physics.wustl.edu
[2] Harvard-Smithsonian Center for Astrophysics, 60 Garden Street, Cambridge, MA 02138, USA
[3] Fred Lawrence Whipple Observatory, Harvard-Smithsonian Center for Astrophysics, Amado, AZ 85645, USA
[4] Department of Physics and Astronomy and the Bartol Research Institute, University of Delaware, Newark, DE 19716, USA
[5] School of Physics, University College Dublin, Belfield, Dublin 4, Ireland
[6] Santa Cruz Institute for Particle Physics and Department of Physics, University of California, Santa Cruz, CA 95064, USA
[7] Argonne National Laboratory, 9700 South Cass Avenue, Argonne, IL 60439, USA
[8] Department of Physics and Astronomy, Iowa State University, Ames, IA 50011, USA
[9] Institute of Physics and Astronomy, University of Potsdam, D-14476 Potsdam-Golm, Germany
[10] DESY, Platanenallee 6, D-15738 Zeuthen, Germany
[11] Astronomy Department, Adler Planetarium and Astronomy Museum, Chicago, IL 60605, USA
[12] School of Physics, National University of Ireland Galway, University Road, Galway, Ireland
[13] Department of Physics and Astronomy, Purdue University, West Lafayette, IN 47907, USA
[14] School of Physics and Astronomy, University of Minnesota, Minneapolis, MN 55455, USA
[15] Department of Astronomy and Astrophysics, 525 Davey Lab, Pennsylvania State University, University Park, PA 16802, USA
[16] Physics Department, McGill University, Montreal, QC H3A 2T8, Canada
[17] Department of Physics and Astronomy, University of Iowa, Van Allen Hall, Iowa City, IA 52242, USA
[18] Department of Physics and Astronomy, University of Utah, Salt Lake City, UT 84112, USA
[19] Department of Physics and Astronomy, DePauw University, Greencastle, IN 46135-0037, USA
[20] Enrico Fermi Institute, University of Chicago, Chicago, IL 60637, USA
[21] Kavli Institute for Cosmological Physics, University of Chicago, Chicago, IL 60637, USA
[22] School of Physics and Center for Relativistic Astrophysics, Georgia Institute of Technology, 837 State Street NW, Atlanta, GA 30332-0430, USA
[23] Department of Life and Physical Sciences, Galway-Mayo Institute of Technology, Dublin Road, Galway, Ireland
[24] Department of Physics and Astronomy, Barnard College, Columbia University, NY 10027, USA
[25] Physics Department, Columbia University, New York, NY 10027, USA
[26] Department of Physics and Astronomy, University of California, Los Angeles, CA 90095, USA
[27] N.A.S.A./Goddard Space-Flight Center, Code 661, Greenbelt, MD 20771, USA
[28] Physics Department, California Polytechnic State University, San Luis Obispo, CA 94307, USA
[29] Department of Applied Physics and Instrumentation, Cork Institute of Technology, Bishopstown, Cork, Ireland
Received 2014 May 17; accepted 2014 June 20; published 2014 July 16

ABSTRACT

The Galactic center is an interesting region for high-energy (0.1–100 GeV) and very-high-energy ($E > 100$ GeV) γ-ray observations. Potential sources of GeV/TeV γ-ray emission have been suggested, e.g., the accretion of matter onto the supermassive black hole, cosmic rays from a nearby supernova remnant (e.g., Sgr A East), particle acceleration in a plerion, or the annihilation of dark matter particles. The Galactic center has been detected by EGRET and by *Fermi*/LAT in the MeV/GeV energy band. At TeV energies, the Galactic center was detected with moderate significance by the CANGAROO and Whipple 10 m telescopes and with high significance by H.E.S.S., MAGIC, and VERITAS. We present the results from three years of VERITAS observations conducted at large zenith angles resulting in a detection of the Galactic center on the level of 18 standard deviations at energies above ∼2.5 TeV. The energy spectrum is derived and is found to be compatible with hadronic, leptonic, and hybrid emission models discussed in the literature. Future, more detailed measurements of the high-energy cutoff and better constraints on the high-energy flux variability will help to refine and/or disentangle the individual models.

Key words: astroparticle physics – black hole physics – Galaxy: center – gamma rays: galaxies – methods: data analysis – radiation mechanisms: non-thermal

Online-only material: color figures

1. INTRODUCTION

The strong radio source Sgr A* located in the center of our galaxy is believed to coincide with a $4 \times 10^6\ M_\odot$ black hole. While molecular clouds and dust hide the view toward the Galactic center at optical wavelengths, transient X-ray events with a 2–10 keV energy output up to 10^{35} erg s^{-1} are observed from Sgr A* on a regular basis (Degenaar et al. 2013; Neilsen

et al. 2013; Barriere et al. 2014), as well as transient events at MeV/GeV energies (Vasileiou et al. 2011). Flares from X-ray binaries located in the Galactic center region can reach luminosities up to 10^{37} erg s^{-1} (Muno et al. 2005; Porquet et al. 2005; Sakano et al. 2005; Wijnands et al. 2006; Degenaar et al. 2012). Various astrophysical sources located close to the Galactic center are potentially capable of accelerating particles to multi-TeV energies, such as the supernova remnant Sgr A East or the pulsar wind nebula (PWN) G 359.95–0.04 (Wang et al. 2006).

A recently discovered gaseous object, G 2, heading toward the immediate vicinity of the Galactic center (Gillessen, et al. 2012) is expected to start merging into the black hole accretion stream some time in 2013–2014. This potential merger is a once-in-a-lifetime event that will allow observers to test magneto-hydrodynamical accretion models and their potential link to emission at the highest energies. Simulations show that the expected change in accretion and emission strongly depend on the origin/properties of the object (Abarca et al. 2014; Ballone et al. 2014; Saitoh et al. 2014) which have not yet been constrained well enough for accurate predictions. The merging process can potentially last for several decades and represents strong motivation for establishing a baseline for the γ-ray emission (as presented here) as well as for ongoing long-term monitoring of this region.

Observations of the Galactic center region also provide an avenue for dark-matter detection (Abramowski et al. 2011). Cold dark matter is widely viewed to be an essential component of the universe in our current standard cosmological model. A 100 GeV to TeV scale thermal relic with weak-scale interactions (or weakly interacting massive particle, WIMP) could provide the cold dark matter required to explain the observed structure in the universe as well as the matter density derived from cosmic microwave background measurements. However, to effectively search for a dark matter annihilation signal in the GeV/TeV regime, it is necessary to first understand the distribution, angular extent, and energy spectrum of the astrophysical sources near the Galactic center.

Several astrophysical sources located in the vicinity of the Galactic center can potentially emit γ-rays at MeV/GeV/TeV energies. Definite associations, on the other hand, are hampered by the limited angular resolution of instruments in these wave bands, ranging from $\simeq$0.1 deg at TeV energies to several degrees in the MeV regime. The EGRET MeV/GeV γ-ray source 3EG J1746-2851 is spatially coincident with the Galactic center (Hartman et al. 1999). More than one MeV/GeV source were resolved by the *Fermi*/LAT instrument (20 MeV $< E \lesssim$ 100 GeV) in the inner $\sim$3 deg region around the Galactic center (Abdo et al. 2010; Nolan et al. 2012), with the strongest source being spatially coincident with the Galactic center (see sky map in Section 3). Uncertainties in the diffuse Galactic background models and the limited angular resolution of the *Fermi*/LAT limits the ability to study the morphologies of these MeV/GeV sources in great detail.

At GeV/TeV energies a detection of a source coincident with the position of the Galactic center was first reported by the CANGAROO II collaboration which operated a ground-based γ-ray telescope in the southern hemisphere. The CANGAROO collaboration reported a steep energy spectrum $dN/dE \propto E^{-4.6}$ (250 GeV $< E \lesssim$ 2.5 TeV) with an integral flux above 250 GeV at the level of 10% of the Crab Nebula flux (Tsuchiya et al. 2004). Shortly after, evidence for emission above 2.8 TeV from the Galactic center at the level of 3.7 standard deviations (s. d.) was reported from 1995 to 2003 large zenith angle (LZA) observations (2.8 TeV $< E \lesssim$ 10 TeV) with the Whipple 10 m γ-ray telescope (Kosack et al. 2004). (See Section 2 for an explanation of LZA observations.)

Observations by H.E.S.S. in 2004–2006 confirmed the Galactic center as a GeV/TeV γ-ray source in the energy range of 100 GeV to several tens of TeV (Aharonian et al. 2004). The measured energy spectrum is described by a power law $dN/dE \propto E^{-2.1}$ with a cutoff at $\sim$15 TeV (Aharonian et al. 2009). No evidence for variability was found in the H.E.S.S. or Whipple data over a time span of more than ten years. The difference between the energy spectrum measured by CANGAROO compared to the spectra measured by the other ground-based GeV/TeV instruments could only be explained if the different instruments observed different astrophysical sources in different states of activity or if the CANGAROO results were affected by a measurement error (see, e.g., Yoshikoshi et al. 2009).

Using the high-precision pointing system of the H.E.S.S. telescopes (reducing the pointing uncertainty to 6″ per axis), the position of the supernova remnant Sgr A East could be excluded as the source of the TeV γ-ray emission (Acero et al. 2010). A diffuse GeV/TeV γ-ray emission was identified after subtracting the point source located at the position of the Galactic center (Aharonian et al. 2006a). Its intensity profile is aligned along the Galactic plane (see sky map in Section 3) and follows the structure of molecular clouds. The energy spectrum of the diffuse emission is described by a power law $dN/dE \propto E^{-2.3}$. It can be explained by an interaction of local cosmic rays (CRs) with the matter in the molecular clouds—indicating a harder spectrum and a higher flux of CRs in this inner region of the Galaxy as compared to the local CR spectrum ($dN/dE \propto E^{-2.7}$) observed at Earth. Recently, an additional, unresolved diffuse component of γ-ray emission was identified by the H.E.S.S. collaboration along the extended Galactic plane (Egberts et al. 2013). The MAGIC collaboration detected the Galactic center in 2004/2005 observations performed at large zenith angles at the level of 7 s. d. (0.5–10 TeV) (Albert et al. 2006), confirming the energy spectrum measured by H.E.S.S.

VERITAS first reported a >10 s. d. detection of the Galactic center in 2010 LZA observations, covering an energy range of 2.5 TeV to several tens of TeV (Beilicke et al. 2011). In this paper, we report on the results of three years (2010–2012) of VERITAS observations of the Galactic center region at large zenith angles at energies above $\sim$2.5 TeV. This paper focuses on the central TeV γ-ray source coincident with the Galactic center. The data were analyzed with the *displacement* method which substantially improves the angular resolution and sensitivity for data taken at large zenith angles (see Section 2). The VERITAS observations and results are discussed in Section 3. A discussion, comparison to models, and prospects of future GeV/TeV γ-ray observations of the Galactic center region are presented in Section 4. A study of the surrounding regions and the dark matter upper limit will be discussed in a second publication.

2. LARGE ZENITH ANGLE OBSERVATIONS

The stereoscopic method of shower reconstruction in ground-based atmospheric Cherenkov telescopes (such as VERITAS) is based on the intersection of the major axes of the parameterized Cherenkov images (Hillas) recorded in individual telescopes (Hofmann et al. 1999). In general, this method is very powerful since it makes use of the full capabilities of the stereoscopic

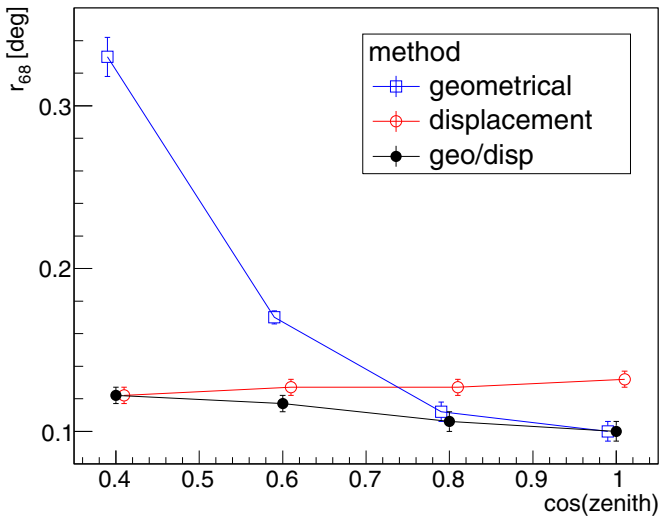

Figure 1. VERITAS angular resolution (68% containment radius r_{68}) as a function of cos(zenith) derived from Monte Carlo simulations with the requirement of at least three images involved in the shower reconstruction. The *geometrical* algorithm performs well for zenith angles $< 40°$ ($\cos(z) > 0.8$) but gets worse for large zenith angles. At zenith angles of 65 deg, the *displacement* method outperforms the *geometrical* algorithm by a factor of more than two. A weighted combination of both algorithms (*geometrical*/*displacement*, see the text) gives an almost flat angular resolution.

(A color version of this figure is available in the online journal.)

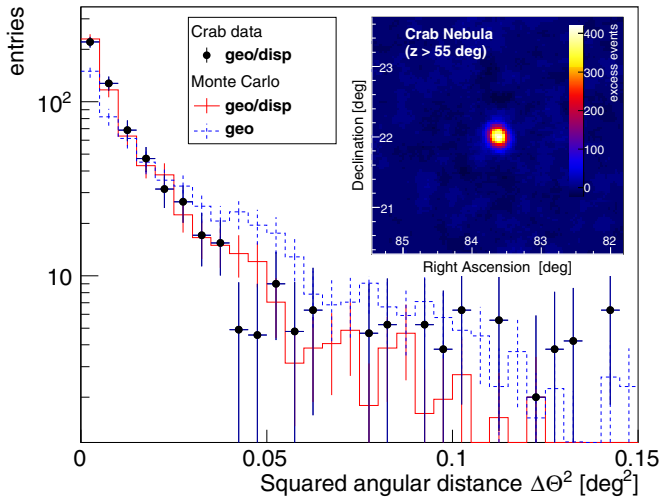

Figure 2. Data points show the angular distribution of excess events from 6.5 hr of Crab Nebula observations taken at zenith angles $z > 55°$. The showers were reconstructed with the combined *geometrical*/*displacement* method. The solid (red) line represents the angular distribution of Monte Carlo events (same reconstruction method) covering the same zenith angle range as the data. The dashed (blue) line shows the distribution of Monte Carlo events which were reconstructed with the standard *geometrical* algorithm. The inlay shows the smoothed excess sky map of the Crab Nebula data (*geometrical*/*displacement* method).

(A color version of this figure is available in the online journal.)

recording of air showers. In the following this method is referred to as the *geometrical* method.

An alternative technique has been developed for data taken with single-telescopes (e.g., Whipple 10 m), using an estimate of the *displacement* parameter which is measured along the major axis of the image between the center of gravity of the Hillas ellipse and the shower position in the camera system (Buckley et al. 1998; Kosack et al. 2004; Domingo-Santamaria et al. 2005). For γ-ray showers the *displacement* parameter has a certain characteristic expectation value (derived from Monte Carlo simulations). Its value can be parameterized as a function of the Hillas parameters (Hillas 1985) of the corresponding image: the length l, the width w, and the amplitude s. Throughout this paper this method is referred to as the *displacement* method.

Large zenith angle observations are observations where the Cherenkov telescopes are pointed to low elevation angles, increasing the average distance to the detected showers. This results in a larger footprint for the Cherenkov lightpool (increasing the effective area), but a decrease of the Cherenkov light intensity also results in an increase of the energy threshold. The larger distance to the shower also decreases the parallactic displacement between images in the different telescopes. Moreover, given the large inclination angle, the angular separation of the telescopes projected into the shower plane are foreshortened in one dimension. The net effect is a strong reduction in the average stereo angle between the major axes of pairs of images, causing a large uncertainty in the determination of the *geometrical* intersection point. This, in turn, leads to a considerable reduction of the angular resolution in the reconstruction of the shower direction and impact parameter. The *displacement* method, on the other hand, does not rely on the intersection of axes, making it independent of the stereo angle between images. Therefore, no substantial drop in performance is expected with increasing zenith angle.

The *displacement* parameter as implemented in the VERITAS analysis (Aliu et al. 2012) was parameterized as a function of l, w, s, the zenith angle z, the azimuth angle Az, as well as the pedestal variance (a measure for readout noise fluctuations) of the image. In contrast to earlier realizations of the method, the parameterization is done in an orthogonal six-dimensional parameter space stored in the form of a lookup table that was trained with an extensive set of Monte-Carlo simulations of γ-ray showers. For each image, the *displacement* parameter is read from the lookup table and results in two most likely points of the shower direction with respect to the image center of gravity (CoG, in camera coordinates): CoG $\pm$ *displacement* along the major axis of the parameterized image. The combination of the points of all images involved in the event resolves the two-fold ambiguity.[30] The reconstruction of the shower impact parameter proceeds in a similar way, again making use of a multi-dimensional lookup table.

Figure 1 shows the angular resolution of both methods (*geometrical* and *displacement*) as a function of the cosine of the zenith angle z, derived from Monte Carlo simulations. While the angular resolution of the *displacement* method remains almost independent of $\cos(z)$, the angular resolution of the standard *geometrical* method becomes increasingly worse at large zenith angles. A further improvement is achieved if both methods are combined: $d = d_{\rm geo} \cdot (1 - w') + d_{\rm disp} \cdot w'$, with the weight being calculated as $w' = \exp(-12.5 \cdot (\cos(z) - 0.4)^2)$ and $w' = 1$ for $\cos(z) < 0.4$, respectively. Both methods benefit in similar ways from an additional requirement of $N \geqslant 3$ images in the event reconstruction. The method was applied to 6.5 hr of LZA Crab Nebula data (Figure 2). The data are in good agreement with the simulations and illustrate the clear improvement the *displacement* method provides in the case of LZA observations. The spectrum reconstructed from the Crab Nebula observations is shown in Figure 5 (in Section 3) and is found to be in reasonable agreement with the H.E.S.S. measurements obtained from lower zenith angles. The LZA Crab data set indicates

[30] Therefore, the method requires $N \geqslant 2$ images to work.

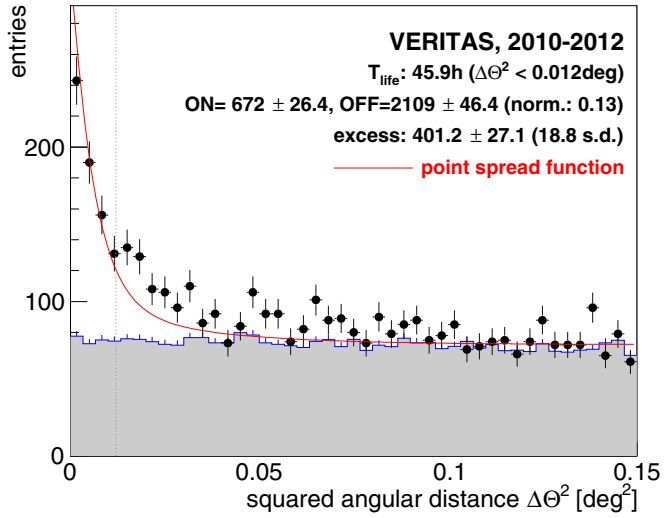

Figure 3. Distribution of the squared angular distance $\Delta\theta^2$ between the reconstructed shower direction and the nominal position of the Galactic center (data points). The distribution is also shown with respect to the events from the reflected OFF regions (shaded area) that are used to determine the background. The red curve represents the point-spread function determined from Monte-Carlo simulations for the corresponding zenith angle interval, normalized to the measured excess determined from the $\Delta\theta^2 \leqslant 0.012\,\mathrm{deg}^2$ regime (vertical dotted line).

an improvement in sensitivity of 30%–40 % when using the combined *displacement*/*geometrical* method compared to the *geometrical* method alone.

3. THE GALACTIC CENTER REGION IMAGED BY VERITAS

VERITAS is an array of four 12 m diameter imaging atmospheric Cherenkov telescopes and is located at the base camp of the Fred Lawrence Whipple Observatory in southern Arizona at an altitude of 1280 m (Holder et al. 2008). VERITAS is sensitive to γ-rays in the energy range of 100 GeV to several tens of TeV. For observations close to zenith, sources of 10% (1%) of the strength and spectrum of the Crab Nebula are detected at the level of 5 s. d. in 0.5 hr (26 hr), respectively.

The Galactic center was observed by VERITAS in 2010–2012 for 46 hr (good quality data, dead-time corrected). Given the declination of the Galactic center, the observations were performed at large zenith angles in the range of $z = 60.2°$–$66.4°$, resulting in an average energy threshold (energy corresponding to the peak detection rate for a Crab-like spectrum) of $E_{\mathrm{thr}} \simeq 2.5$ TeV. The shower direction and impact parameter were reconstructed with the *geometrical*/*displacement* method as described in Section 2. Other than using the *displacement* method, the standard analysis procedure was applied with event selection cuts a priori optimized for weak, hard-spectrum sources: angular separation between source position and reconstructed shower direction of $\Delta\theta^2 \leqslant 0.012\,\mathrm{deg}^2$, mean scaled width/length $\leqslant 1.04/1.25$, and $N \geqslant 3$ images per event.

In the case of ground-based Cherenkov astronomy, the atmosphere acts as a calorimeter and its influence on the transmission of Cherenkov light is the single largest contributor to the systematic uncertainty in the estimate of the reconstructed TeV γ-ray energy E. The overall uncertainty for close-to-zenith observations is estimated to be on the order of $\Delta E/E \simeq 0.2$, with an atmospheric contribution of about 0.15. For a spectrum $dN/dE \propto E^{-2.5}$, this translates into an error in flux of $\Delta\Phi/\Phi \simeq 0.2$. The column density of the atmosphere changes with $1/\cos(z)$ and, conservatively, the systematic error in the energy/flux reconstruction can be expected to scale accordingly. For the Galactic center observations the contribution of the systematic effect induced by the atmosphere therefore roughly doubles as compared to low-zenith angle observations and we estimate the systematic error on the LZA flux normalization to be $\Delta\Phi/\Phi \simeq 0.4$.

This section describes the results of the TeV γ-ray source coincident with the Galactic center. In the three-year data set, an excess on the order of 18 s. d. is found at the position of Sgr A* (see Figure 3). The background for the excess study (as well as for the energy spectrum, see below) was estimated from seven regions placed at the same radial camera distance as the source region (reflected background model, see Berge et al. 2007). The tail in the angular excess distribution can likely be explained by a contribution from the surrounding diffuse emission (Aharonian et al. 2006a) which becomes increasingly important at higher energies (Viana & Moulin 2013). More detailed studies on the diffuse emission morphology will be presented in a second paper.

Figure 4 shows the VERITAS sky map of the Galactic center region. The background in this figure was estimated

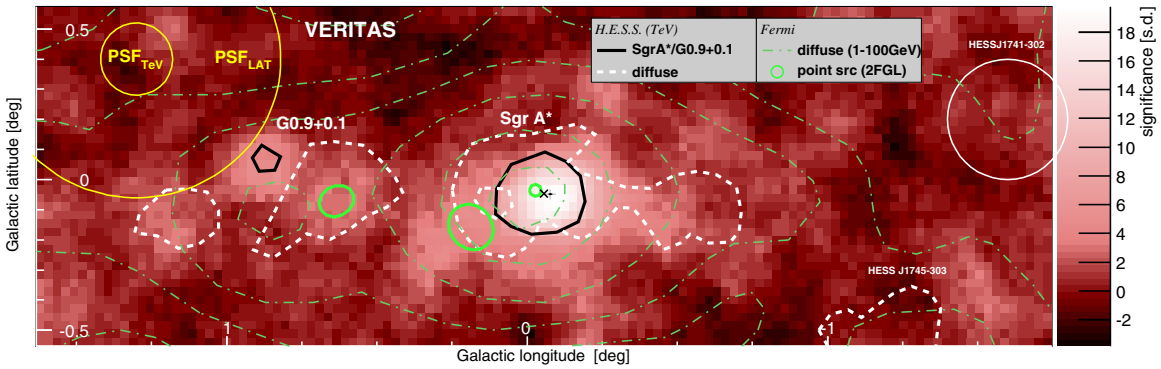

Figure 4. VERITAS sky map of the Galactic center region (smoothed excess significances, ring background model). The VERITAS centroid position is indicated by the cross (statistical and systematic errors) and the Sgr A* radio position is indicated by the "x". The solid black contour lines indicate the Galactic center and the supernova remnant G 0.9+0.1 as seen by H.E.S.S. (Aharonian et al. 2004). The white dashed contour lines indicate the H.E.S.S. diffuse emission along the Galactic plane and from HESS J1745-303 (Aharonian et al. 2006a). The position of HESS J1741–302 is indicated by the labeled circle. The green solid ellipses indicate the positions of the MeV/GeV sources and their 95% position errors taken from the second *Fermi*/LAT catalog (Nolan et al. 2012). The green dash-dotted contour lines indicate the 1–100 GeV diffuse emission (after subtracting point-sources, Galactic, and extragalactic backgrounds) as measured by *Fermi*/LAT (Yusef-Zadeh et al. 2013). The instruments' point spread functions (68% containment radius) of VERITAS and *Fermi*/LAT (1–100 GeV, calculated for the 2FGL log parabola spectrum of the source coincident with SgrA*) are indicated in the upper left corner.

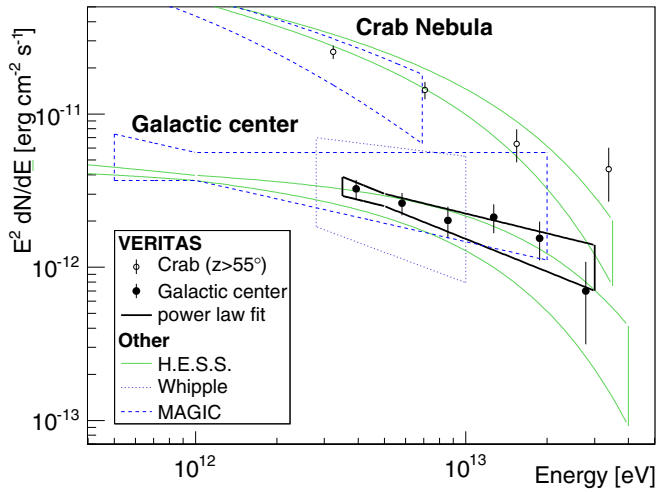

Figure 5. VERITAS energy spectra shown for LZA observations of the Crab nebula and the Galactic center (statistical errors only). Also indicated are the fit results of the spectra measured by Whipple (dotted bow tie, Kosack et al. 2005), H.E.S.S. (solid bow ties, Aharonian et al. 2006b, 2009), and MAGIC (dashed bow ties, Albert et al. 2008, 2006).

(A color version of this figure is available in the online journal.)

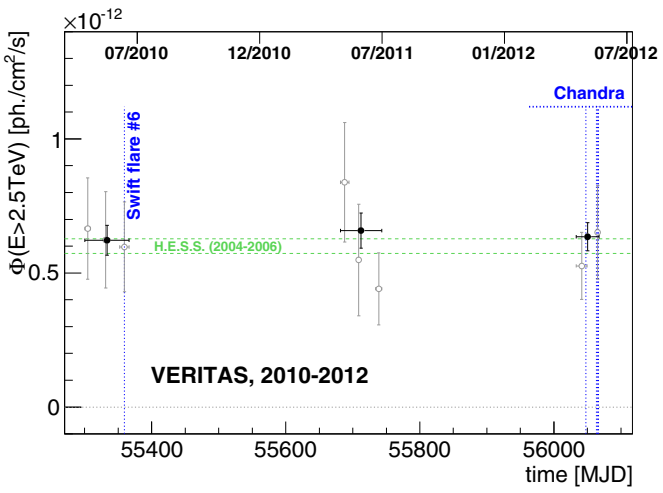

Figure 6. Integral flux above 2.5 TeV from the direction of the Galactic center on a month-by-month basis (open points), as well as the yearly averages (solid points). The time of the X-ray flare #6 detected by *Swift* (Degenaar et al. 2013) is indicated. The period of X-ray *Chandra* observations of Sgr A* (Neilsen et al. 2013) is shown as the dotted horizontal line. VERITAS synchronized four observations with the *Chandra* pointings (same day, vertical lines). The dashed horizontal lines indicate the statistical error range of the 2004–2006 average TeV γ-ray flux which was derived by integrating the H.E.S.S. spectrum shown in Figure 5 for $E > 2.5$ TeV.

(A color version of this figure is available in the online journal.)

using a ring-like region ($0.^\circ45 \leqslant r \leqslant 0.^\circ7$) surrounding each test position (ring background model, see Berge et al. 2007), with a correction term taking into account the camera acceptance. Both background models exclude known sources from the background estimate (HESS J1741-302, HESS J1745-303, G 0.9+0.1, and the Galactic center itself). A fit of the point spread function to the uncorrelated excess sky map results in a centroid position of the excess in Galactic coordinates of long $= (-0.077 \pm 0.006_{\rm stat} \pm 0.013_{\rm sys})$ deg and lat $= (-0.049 \pm 0.003_{\rm stat} \pm 0.013_{\rm sys})$ deg with a fit quality of $\chi^2/{\rm d.o.f.} = 77.1/61$. We name the VERITAS source VER J1745-290. This position is compatible with the Galactic center position (long $= -0.^\circ056$ and lat $= -0.^\circ046$) and the position measured by H.E.S.S. Both positions are indicated in Figure 4 which also shows the contour lines of the diffuse emission measured by H.E.S.S. (Aharonian et al. 2006a). Furthermore, Figure 4 shows the positions of the MeV/GeV sources taken from the 2FGL *Fermi* catalog (Nolan et al. 2012), as well as the contour lines of the 1–100 GeV diffuse emission after subtraction of point sources, extragalactic, and Galactic backgrounds (Yusef-Zadeh et al. 2013).

The VERITAS energy spectrum obtained from the three-year data set is shown in Figure 5 and is found to be compatible with the spectra measured by Whipple (Kosack et al. 2005), H.E.S.S., and MAGIC. It can be described ($\chi^2/{\rm dof} = 2.1/4$) by a power law $dN/dE = I_0(E/5\,{\rm TeV})^{-\Gamma}$ with a normalization at the decorrelation energy of 5 TeV of $I_0 = (6.89 \pm 0.64_{\rm stat} \pm 2.75_{\rm syst})\,10^{-14}$ photons cm^{-2} s^{-1} TeV^{-1} and a photon index of $\Gamma = 2.57 \pm 0.14_{\rm stat} \pm 0.2_{\rm syst}$. Since the LZA effective area of the VERITAS observations compensates for the shorter exposure (46 hr) as compared to the low-zenith H.E.S.S. observations (93 hr), the statistical errors of the VERITAS $E > 2.5$ TeV data points are comparable to those of the H.E.S.S. measurements. Recently, the H.E.S.S. collaboration reported an updated energy spectrum that was corrected for the energy-dependent contribution from the surrounding diffuse emission, leading to a lower cutoff energy around 10 TeV (Viana & Moulin 2013).

The night-by-night integral fluxes above 2.5 TeV are calculated by folding a fixed spectral slope (derived from the energy spectrum for the full data set: $dN/dE \propto E^{-2.6}$) with the effective area for the zenith angle of the corresponding night and comparing it with the excess counts above the threshold found in the data. The fluxes were binned according to observation periods of ~3 week duration (as summarized in Table 1) and are shown in Figure 6 together with the yearly integral fluxes obtained from integrating the reconstructed energy spectra obtained for the individual years. No evidence for flux variability was found in the three-year data (the fit of a constant function to the run-by-run light curve (20 min segments) yields a fit quality of $\chi^2/{\rm dof} = 117/150$). The H.E.S.S. collaboration reported a fit quality of $\chi^2/{\rm dof} = 233/216$ as a result of a comparable study based on their 2004–2006 data set divided into 28 min segments (Aharonian et al. 2009).

Table 1
The Time Spans (MJD) of the Individual Observation Periods (Gray Data Points in Figure 6)

Year	Begin (MJD)	End (MJD)
2010	55300.4	55308.4
	55328.3	55334.4
	55352.3	55366.3
2011	55681.4	55694.4
	55707.3	55710.4
	55734.2	55743.3
2012	56033.4	56049.5
	56063.3	56067.4

Note. Observations were not performed continuously within each period, but were spread out in 20–60 minutes data segments in individual nights.

4. DISCUSSION

4.1. VERITAS Results in the Context of Multi-wavelength Data

The following potential counterparts are located[31] within the $1'$ position uncertainty (statistical plus systematic) of the

[31] http://simbad.u-strasbg.fr

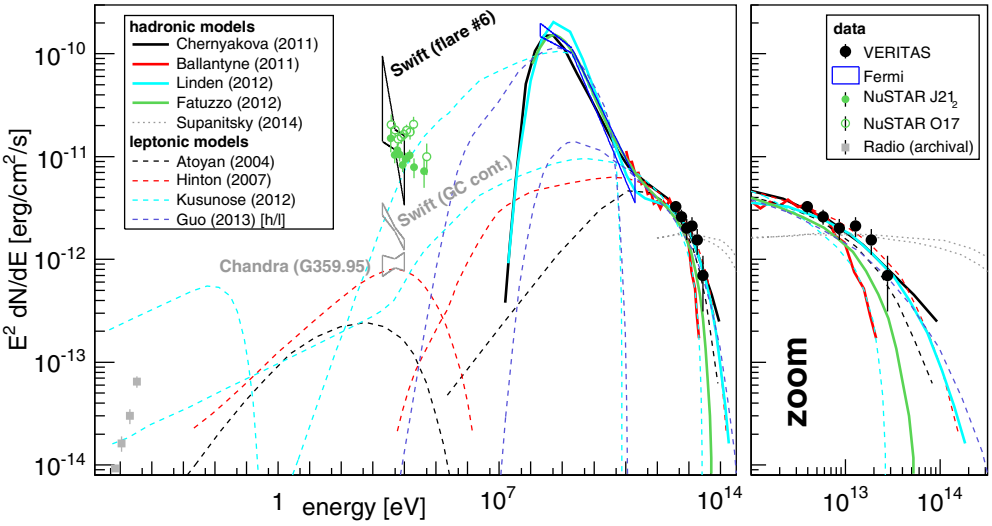

Figure 7. Left: VERITAS spectral energy distribution of the Galactic center point-source compared to hadronic and leptonic emission models as discussed in the text. The *Fermi*/LAT bow tie is taken from Chernyakova et al. (2011). The multi-wavelength data points shown are archival radio (Davies et al. 1976), X-ray flares observed by *Swift* (Degenaar et al. 2013) and NuSTAR (Barriere et al. 2014), as well as flux measurements from *Chandra* (Wang et al. 2006). Right: zoomed version of the TeV regime.

VERITAS excess: (1) the Galactic center Sgr A*, (2) the supernova remnant Sgr A East, (3) the PWN G 359.95–0.04, (4) the low mass X-ray Binary AX J1745.6−2901, (5) nine maser objects, and (6) about 150 X-ray sources. Here, (1)–(3) have the highest potential for TeV γ-ray emission. Sgr A East, however, was excluded as TeV counterpart by H.E.S.S. (Acero et al. 2010). PWN G 359.95−0.04 is discussed as potential counterpart in Section 4.2. In general, a contribution to the measured TeV γ-ray flux from more than one object cannot be excluded.

Sgr A* is known to exhibit 2–10 keV X-ray flares above the quiescent level on a regular basis, as for example observed in the 2006–2011 *Swift* monitoring campaign (Degenaar et al. 2013). A bright X-ray flare (flare #6, MJD 55359) was detected by *Swift* during the 2010 VERITAS monitoring but no TeV data were taken on that particular night. The time of the X-ray flare is indicated in Figure 6 and its spectrum is shown in the spectral energy distribution (SED) in Figure 7 together with a baseline measurement of the continuum emission from the extended region surrounding the Galactic center (including the contribution of Sgr A*). High spatial resolution X-ray observations were conducted in 2012 by *Chandra* (Neilsen et al. 2013) for a total of 3 Ms leading to the detection of 39 X-ray flares from the Galactic center with durations ranging from $O(100\,\mathrm{s})$ to $O(8\,\mathrm{ks})$. The observed flare luminosities in the 2–10 keV band reached 10^{34} to $2\times10^{35}\,\mathrm{erg\,s^{-1}}$. The time span of the *Chandra* campaign is indicated in Figure 6, where four nights had quasi-simultaneous coverage (same night) by VERITAS. Medium-intensity X-ray flares were detected in two out of those four nights at MJD 56047.7 and 56066.4. However, no significant flux changes were observed in the TeV band (see Section 4.4 for an estimate of the VERITAS sensitivity to detect variability). In an earlier campaign an X-ray flare was observed during joint H.E.S.S./*Chandra* observations in 2005; but no increase in TeV γ-ray flux was measured (Hinton et al. 2008).

One possible origin of the observed X-ray flares is a change/disruption in accretion rate. In models where the TeV emission comes from particle acceleration near the black hole, one might expect some connection between the variation in the X-ray emission of the accretion and the TeV γ-ray production (see next section). The frequency of X-ray flares exceeding the quiescent state by a factor of 10 is estimated to be roughly one flare per day (Neilsen et al. 2013). The frequency of bright ($L_X > 10^{35}\,\mathrm{erg\,s^{-1}}$) X-ray flares is estimated to be 0.1–0.2 per day (Degenaar et al. 2013). Given (1) the sensitivity of the VERITAS LZA Galactic center observations, (2) the X-ray flare intensity and (3) flare frequency, it is challenging to correlate (with either direct or delayed response functions) the two wave bands on the basis of individual flares unless much stronger X-ray flares are observed ($\gg$10 times the X-ray quiescent level). Most TeV emission models (see next section) predict a "smoothing out" of the accretion/flare activity in the TeV response, if there is any relationship at all.

Four more medium-intensity X-ray flares with durations of less than one hour and energies reaching up to 79 keV were detected in a NuSTAR campaign conducted in summer/fall 2012 (Barriere et al. 2014). Although the VERITAS 2012 observations had already ended by that time, the measured spectra of the two strongest flares J21$_2$ (07/2012) and O17 (10/2012) are shown in Figure 7 for reference.

At current times the emission level from the Galactic center is roughly 10 orders of magnitude below its Eddington luminosity (Terrier et al. 2010; Sunyaev et al. 1993). Spatial and temporal variations in the X-ray flux measured from molecular clouds surrounding the Galactic center have been found (Terrier et al. 2010; Ponti et al. 2010; Sunyaev et al. 1993). The results are interpreted as a bright $10^{39}\,\mathrm{erg\,s^{-1}}$ outburst of a source coincident with Sgr A* that happened $O(100)$ yr ago. These findings indicate long-term variations in accretion/brightness of the central source (Ponti et al. 2010). Recently, the Fermi/LAT instrument discovered two large γ-ray bubbles extending below and above the Galactic center (Su et al. 2010). Although the origin of the bubbles remains unclear so far, a significant increase in energy injection from the Galactic center on timescales of Myr is discussed as one of the possibilities (Su et al. 2010); for example, in the form of a plasma jet originating from the (previously brighter) active galactic nucleus in our galaxy (Yang et al. 2013; Guo et al. 2012).

4.2. Comparison to Models

A variety of astrophysical models have been proposed to explain the GeV/TeV γ-ray emission from the Galactic center region. This section discusses a selection of leading models that cover the range of viable hypotheses. The models are shown together with the VERITAS and multi-wavelength data in Figure 7. Most of the models were tuned based on the H.E.S.S. results so that a general agreement with the VERITAS spectrum is not surprising. While some of these models link accretion onto the black hole to the X-ray and γ-ray data, most of them find a way to address the lack of variability in the TeV emission, and a direct flux correlation between the X-ray/TeV band is not predicted. With respect to the TeV γ-ray emission, models can be divided into two broad classes: hadronic models or leptonic models depending on which species of energetic particles dominates the γ-ray emission.

4.2.1. Hadronic Models

Most of the hadronic acceleration models such as Chernyakova et al. (2011) and Ballantyne et al. (2011) explain the emission by the following mechanism: (1) protons are being accelerated in the black hole vicinity at distances of up to a few tens of Schwarzschild radii. (2) The accelerated protons diffuse out into the interstellar medium where they (3) undergo nuclear interactions and produce neutral pions which decay into GeV/TeV γ-rays: $\pi^0 \rightarrow \gamma\gamma$. The spectral break between the MeV/GeV and TeV spectra is explained by a strong energy dependence of the diffusion coefficient separating the high-energy particles into two different diffusion regimes (Chernyakova et al. 2011). Changes in the TeV flux can potentially be caused by changes in the black hole vicinity (e.g., accretion) but will not manifest themselves instantaneously. The time scales of flux variations in these models are $\sim 10^4$ yr at MeV/GeV energies (old flares) and $\sim$10 yr at $E > 10$ TeV ("new" flares caused by recently injected high-energy particles). Significant spectral variability has not been seen but is also not strongly constrained following $\sim$15 years of observations by Whipple, H.E.S.S., MAGIC, and VERITAS. However, such variability can be expected in this model for $E > 10$ TeV with the TeV spectrum softening following an outburst (Ballantyne et al. 2011). Constraining the $E > 10$ TeV spectral variability would serve as an important test for this class of models (see Section 4.4 for an estimate of the VERITAS sensitivity to constrain flux variability). Linden et al. (2012) discuss the surrounding gas as a proton target that defines the morphology of the TeV γ-ray emission.

Fatuzzo & Melia (2012) interpret the inflected structure in the GeV/TeV spectrum as a hint for an energizing process more complicated than typical nonrelativistic diffusive shock acceleration. While questioning some of the assumptions made by Chernyakova et al. (2011) their model assumes a steady-state cosmic-ray ejection by Sgr A* without a particle diffusion coefficient that strongly depends on energy. Their model treats the inner parsecs of the galaxy as a uniform *wind zone* (interactions of stellar winds from the surrounding young stars) that encompasses a high-density *molecular torus* with an inner radius of 1.2 pc and a thickness of 1 pc. The high-energy tail of the thermal proton distribution near the black hole serves as a seed population for the stochastic acceleration process. The γ-rays are produced via π^0 decays or electromagnetic $\pi^{\pm}$ cascades as a consequence of pp scattering. In this scenario the emission observed in the *Fermi*/LAT band is dominated by scattering in the torus whereas the TeV emission is dominated by scattering in the wind zone.

Motivated by the recent IceCube detection of five $E > 30$ TeV neutrinos from the direction of the Galactic center region (Aartsen et al. 2013), Supanitsky (2014) studies the interaction of cosmic ray protons (1) accelerated by sources in the Galacic center region, (2) interacting with ambient protons, and (3) calculates the resulting γ-ray and neutrino spectra. It should be stressed that Supanitsky (2014) discusses a hypothetical PeV cosmic ray accelerator (Pevatron) located in the Galactic center region, which has no experimental evidence for its existence so far. Not surprisingly, the predicted spectrum differs substantially from the models discussed above and can be constrained by more sensitive observations at the highest energies.

4.2.2. Leptonic Models

Atoyan & Dermer (2004) discuss a black hole plerion model. Here, a magnetized leptonic wind originates from the advection dominated accretion flow surrounding the black hole and results in a termination shock located at a distance of 3×10^{16} cm ($\simeq$7500 Schwarzschild radii) from the black hole. The shock accelerates leptons to relativistic energies which in turn produce TeV γ-rays via inverse Compton scattering. This model fails to explain the flux in the MeV/GeV regime (Figure 7). However, given the limited angular resolution, the emission observed in the *Fermi*/LAT band may well originate from a different region, different source, or a different spectral component in the same source. Future *Fermi*/VERITAS flux correlation studies will serve as crucial experimental inputs to understand a possible common versus separate origin of these two SED components. The hadronic models, on the other hand, can explain the MeV/GeV part of the SED by the superposition of different flare stages that occurred in the recent history of the source. The flux variability time scale in Atoyan & Dermer (2004) is on the order of $T_{\rm var} \sim 100$ yr and therefore provides a prediction that would be falsified by the detection of TeV γ-ray flux variability.

Kusunose & Takahara (2012) discuss a leptonic model that involves a different location/mechanism for the MeV/GeV versus TeV emission. The observed (quasi-continuous) X-ray flaring is seen as synchrotron emission of non-thermal electrons that are injected and accumulate in a region of $r \leqslant 10^{18}$ cm ($\simeq 7.5 \times 10^5$ Schwarzschild radii) around the black hole. These electrons produce MeV/GeV γ-rays seen by *Fermi*/LAT via inverse Compton scattering off soft star/dust photons.[32] By increasing the electron Lorentz factor and reducing the injection rate, the model can be tuned to describe the TeV emission as well. However, it cannot describe the MeV/GeV and TeV emission with a single set of model parameters suggesting different origins or emission zones of the two measured spectral components.

Hinton & Aharonian (2007) link the TeV emission to the recently discovered pulsar wind nebula G 359.95–0.04 (Wang et al. 2006) located only 0.3 pc (projected) away from the Galactic center. The authors adjust the PWN/TeV scenario to the very high density of low-frequency radiation found in the particular region of the Galactic center. This environment leads to a hardening of the high-energy electron spectrum and to more efficient TeV emission as compared to the same PWN located in a "regular" environment. The model does not describe the *Fermi*-observed MeV/GeV spectrum which in this scenario would originate from a different location. Given the instruments' point spread functions (VERITAS: $\simeq 0.^{\circ}1$, *Fermi*/LAT: $\simeq 0.^{\circ}5$

[32] The model versus data difference in the radio regime is explained by a difference in emission regions considered versus measured.

at 1–100 GeV, $\simeq 2.^{\circ}5$ at 100 MeV–1 GeV), neither *Fermi* nor VERITAS is capable of distinguishing between the positions of G 359.95−0.04 and the Galactic center based on the measured excess location.

It should be noted that the $E > 10$ TeV leptonic emission in the models discussed above is strongly Klein–Nishina suppressed in the case of photon fields with temperatures above 100 K.

4.2.3. Hybrid Models

Guo et al. (2013) discuss a hybrid model that assumes simultaneous acceleration of hadrons and electrons during a past phase of activity of the Galactic center and significant contributions to the observed SED by both hadronic and leptonic radiative processes. The particles are accelerated in a region surrounding the black hole, with a radius of approximately 10 Schwarzschild radii, diffuse outward, and interact with interstellar gas and radiation fields, respectively. In this scenario the hadrons are responsible for the TeV emission via the π^0 decay channel from a region with $r < 3$ pc. Fast cooling electrons, on the other hand, would dominate the MeV/GeV emission via inverse Compton scattering off the soft background photons in a region with $r < 1.2$ pc. The cutoff in the MeV/GeV spectrum moves toward lower energies and the spectrum softens with increasing time since particle injection activity. The time dependence of the TeV spectrum is weaker, with a softening trend in time. Both spectral components drop in flux by roughly a factor of two within $O(100\,\mathrm{yr})$. Within this framework, the measured MeV/GeV and TeV spectra can be simultaneously explained by a 10^{48} erg injection event roughly 200 yr ago. The authors note that an outburst similar to the one observed by *Chandra* in 2012 would lead to TeV emission three orders of magnitude below the current measurements—implying that much stronger past activity was responsible for the current state of MeV/GeV/TeV emission.

4.3. Prospects for Dark Matter Limits

A number of extensions to the standard model of particle physics predict new particles with TeV-scale masses. Supersymmetry, e.g., provides a natural candidate for WIMP dark matter, the neutralino or lightest (stable) sypersymmetric particle. If these WIMPs were thermal relics, their interactions in the early universe imply that they will interact with ordinary matter in the present, annihilating to form standard model particles and γ-rays or, in some cases, even decaying.

In almost any scenario of cold dark matter structure formation, the Milky Way halo is thought to be peaked in the Galactic center region and the annihilation rate, proportional to the density squared, would be even more strongly peaked near the Galactic center. WIMPS could annihilate directly to γ-rays forming narrow lines (through $\chi\chi \rightarrow \gamma\gamma$ or $\chi\chi \rightarrow \gamma + Z^0$) or annihilate to quarks or heavy leptons, hadronizing and producing secondary γ-rays in a continuum (Jungman et al. 1996). The resulting spectrum would have a cut-off near the WIMP mass m_χ, as well as a detailed spectral shape determined by the annihilation channel.

Prior to the LHC, the natural mass for WIMPs was thought to fall below TeV energies, the energy range previous searches had been focusing on (see e.g., Abramowski et al. 2011). But with recent constraints from the LHC, multi-TeV scale WIMPs have attracted increasing attention (Livio & Silk 2014). Above a few TeV, nonperturbative effects (e.g., Sommerfeld enhancements from W or Z exchange) could boost the annihilation cross-section by more than an order of magnitude. Thus, multi-TeV measurements of γ-ray emission from the Galactic center are of great interest. The study of diffuse emission and upper limits on a dark matter annihilation signal will follow this paper that first identifies astrophysical point sources.

4.4. Prospects of Future VERITAS Observations

As discussed in Section 4.2, most of the emission models start to differ in the cutoff regime around 10 TeV (see Figure 7). Furthermore, some of the hadronic models predict variability in the $E > 10$ TeV flux on timescales of $O(10\,\mathrm{yr})$ whereas the leptonic model family predicts flux changes on time scales not shorter than $O(100\,\mathrm{yr})$. The differences are to a large extent the result of different assumptions concerning the acceleration rates (and sizes of the emission regions): the hadronic models assume abrupt changes in acceleration whereas the leptonic models assume much slower variations in the acceleration rate. Future VERITAS observations would help to constrain the different models by having a more accurate measurement of the cutoff energy, as well as better constraints on the time variability of the emission.

In the data set presented in this paper, VERITAS detects emission from the direction of the Galactic center above 10 TeV at a significance level of 7.5 s. d. with a rate of 1.1 s. d. per $\sqrt{\mathrm{h}}$. Assuming a continuation of the monitoring of 15 hr per year the change in $E > 10$ TeV flux can be constrained as follows. Assuming an increase in the flux of 0/50/100% the VERITAS detection within individual years would result in excess significances of 4.4/6.7/8.8 s. d., respectively. The doubling of the flux from one year to another could be detected at the level of 3.4 s. d. An increase by a factor of three would be highly significant (5 s. d.). An estimate of the corresponding sensitivity for flux changes in the whole energy range covered by the VERITAS observations ($E \gtrsim 2.5$ TeV) would result in the detection of a 40% increase in flux from one year to another at the level of 5.5 s. d.

The X-ray flares observed by *Swift*, *Chandra*, and NuSTAR can reach flux amplitudes of more than one order of magnitude above the X-ray quiescence level. Although the TeV emission models discussed in Section 4.2 do not predict a direct link, it is important to constrain/exclude X-ray/TeV flux correlations (e.g., X-ray flares may mark a different mechanism that potentially could be accompanied by direct TeV $\gamma - ray$ emission). Assuming a comparable increase in X-ray versus TeV flux, VERITAS would be able to establish the corresponding flux variability at a high level of significance. However, the X-ray flares only last for short timescales of $O(1\,\mathrm{hr})$ so that exactly simultaneous X-ray/TeV observations are required during a strong X-ray flare to test a possible correlation.

Another strong motivation for a continuation of the TeV monitoring of the Galactic center region is the gaseous object G 2 heading toward its center (Gillessen, et al. 2012). Although the predictions for the changes in accretion rate vary (but will be further constrained by ongoing multi-wavelength campaigns in the years to come), this event marks a unique opportunity in which well-defined changes of the environment conditions of the black hole vicinity can be used to study the corresponding impacts on non-thermal emission in the X-ray band and up to MeV/GeV/TeV energies. Although the TeV flux will in most models react to changes in accretion on timescales $\gg 1$ yr, short-term changes in the high-energy regime by local shock acceleration due to the merging process cannot be excluded.

Observations in the GeV/TeV regime with the next-generation instrument, the Cherenkov Telescope Array (CTA Consortium 2010), will be almost one order of magnitude more sensitive and will be well-suited for more detailed variability studies.

As of the beginning of 2014 the ongoing radio monitoring with the VLA did not yet reveal a significant brightening of the Galactic center region due to the merger (Chandler & Sjouwerman 2014). However, the process of merging is believed to last for several decades, with inaccurate predictions so far about its exact onset.

5. SUMMARY AND CONCLUSIONS

The implementation of the *displacement* method in the VERITAS data analysis chain has substantially improved the shower reconstruction and sensitivity for data taken at large zenith angles. It allows detection of the Galactic center at the level of 5 s. d. in roughly 3 hr with $z > 60^\circ$ observations. The measured energy spectrum is found to be in agreement with earlier measurements by H.E.S.S., MAGIC, and Whipple. At energies above 2.5 TeV the VERITAS measurements are competitive with H.E.S.S. Further constraints on emission models can be placed by future observations to measure the cutoff energy in the spectrum and to determine limits on the flux variability at the highest energies. The recently discovered gaseous object G 2 heading toward the immediate vicinity of the Galactic center black hole (Gillessen, et al. 2012) represents further motivation for future TeV γ-ray monitoring of this region. In addition to the potential for discoveries, the observations will establish a base line TeV γ-ray flux and spectrum that can be used to study possible changes caused by the merging process that can potentially last for several decades (Abarca et al. 2014; Ballone et al. 2014; Saitoh et al. 2014). An upper limit on diffuse γ-ray emission surrounding the Galactic center region and, in consequence, a limit on the photon flux initiated by the annihilation of dark matter will be presented in a separate publication.

This research is supported by grants from the U.S. Department of Energy Office of Science, the U.S. National Science Foundation, and the Smithsonian Institution, by NSERC in Canada, by Science Foundation Ireland (SFI 10/RFP/AST2748) and by STFC in the UK. We acknowledge the excellent work of the technical support staff at the Fred Lawrence Whipple Observatory and at the collaborating institutions in the construction and operation of the instrument.

REFERENCES

Aartsen, M. G., Abbasi, R., Abdou, Y., et al. 2013, Sci, 342, 1242856
Abarca, D., Sadowski, A., & Sironi, L. 2014, MNRAS, 440, 1125
Abdo, A. A., Ackermann, M., Ajello, M., et al. 2010, ApJS, 188, 405
Abramowski, A., Acero, F., Aharonian, F., et al. 2011, PhRvL, 106, 161301
Acero, F., Aharonian, F., Akhperjanian, A. G., et al. 2011, MNRAS, 402, 1877
Aharonian, F. A., Akhperjanian, A. G., Anton, G., et al. 2009, A&A, 503, 817
Aharonian, F. A., Akhperjanian, A. G., Aye, K.-M., et al. 2004, A&A, 425, L13
Aharonian, F. A., Akhperjanian, A. G., Bazer-Bachi, A. R., et al. 2006a, Natur, 439, 695
Aharonian, F. A., Akhperjanian, A. G., Bazer-Bachi, A. R., et al. 2006b, A&A, 457, 899
Albert, J., Aliu, E., Anderhub, H., et al. 2006, ApJL, 638, L101
Albert, J., Aliu, E., Anderhub, H., et al. 2008, ApJ, 674, 1037
Aliu, E., Archambault, S., Arlen, T., et al. 2012, ApJ, 754, 77
Atoyan, A., & Dermer, C. D. 2004, ApJL, 617, L123
Ballantyne, D. R., Schumann, M., & Ford, B. 2011, MNRAS, 410, 1521
Ballone, A., Schartmann, M., Burkert, A., et al. 2014, IAUS, 303, 307
Barriere, N. M., Tomsick, J. A., Baganoff, F. K., et al. 2014, ApJ, 786, 46
Beilicke, M., Aliu, E., Archambault, S., et al. 2011, in Proc. Fermi Symp., ed. A. Morselli, arXiv:1109.6836
Berge, D., Funk, S., & Hinton, J. 2007, A&A, 466, 1219
Buckley, J. H., Akerlof, C. W., Carter-Lewis, D. A., et al. 1998, A&A, 329, 639
Chandler, C. J., & Sjouwerman, L. O. 2014, Atel, 6247, see also https://science.nrao.edu/science/service-observing
Chernyakova, M., Malyshev, D., Aharonian, F. A., Crocker, R. M., & Jones, D. I. 2011, ApJ, 726, 60
CTA Consortium 2010, arXiv:1008.3703
Davies, R. D., Walsh, D., & Booth, R. S. 1976, MNRAS, 177, 319
Degenaar, N., Miller, J. M., Kennea, J., et al. 2013, ApJ, 769, 155
Degenaar, N., Wijnands, R., Cackett, E. M., et al. 2012, A&A, 545, 49
Domingo-Santamaria, E., Flix, J., Rico, J., Scalzotto, V., & Wittek, W. 2005, Proc. ICRC, 5, 363
Egberts, K., Brun, F., Casanova, S., et al. 2013, ICRC, eprint (arXiv:1308.0161)
Fatuzzo, M., & Melia, F. 2012, ApJ, 757, 16
Gillessen, S., Genzel, R., Fritz, T., et al. 2012, Natur, 481, 51
Guo, F., & Mathews, W. G. 2012, ApJ, 756, 181
Guo, Y.-Q., Yuan, Q., Liu, C., & Li, A.-F. 2013, JPhG, 40, 5201
Hartman, R. C., Bertsch, D. L., Bloom, S. D., et al. 1999, ApJS, 123, 79
Hillas, A. M. 1985, in NASA Goddard Space Flight Center 19th Int. Cosmic Ray Conf., Vol. 3, 445
Hinton, J. A., & Aharonian, F. A. 2007, ApJ, 657, 302
Hinton, J. A., Vivier, M., Bühler, R., et al. 2005, ICRC, 2, 633
Hofmann, W., Jung, I., Konopelko, A., et al. 1999, APh, 12, 135
Holder, J., Acciari, V. A., Aliu, E., et al. 2008, in AIP Conf. Proc. 1085, Proc. 4th Int. Meeting on High Energy Gamma-Ray Astronomy, ed. F. A. Aharonian, W. Hofmann, & F. Rieger (Melville, NY: AIP), 657
Jungman, G., Kamionkowski, M., & Griest, K. 1996, PhR, 267, 195
Kosack, K. P. 2005, PhD thesis, Washington Univ. St.Louis
Kosack, K. P., Badran, H. M., Bond, I. H., et al. 2004, ApJ, 608, 97
Kusunose, M., & Takahara, F. 2012, ApJ, 748, 34
Linden, T., Lovegrove, E., & Profumo, S. 2012, ApJ, 753, 41
Livio, M., & Silk, J. 2014, Natur, 507, 29
Muno, M. P., Lu, J. R., Baganoff, F. K., et al. 2005, ApJ, 633, 228
Neilsen, J., Nowak, M. A., Gammie, C., et al. 2013, in IAU Sym. 303, The Galactic Center: Feeding and Feedback in a Normal Galactic Nucleus (Cambridge: Cambridge Univ. Press), arXiv:1311.6818
Nolan, P. L., Abdo, A. A., Ackermann, M., et al. 2012, ApJS, 199, 31
Ponti, G., Terrier, R., Goldwurm, A., Bélanger, G., & Trap, G. 2010, ApJ, 714, 732
Porquet, D., Grosso, N., Burwitz, V., et al. 2005, A&A, 430, 9
Saitoh, T. R., Makino, J., Asaki, Y., et al. 2014, PASJ, 66, 1
Sakano, M., Warwick, R. S., Decourchelle, A., & Wang, Q. D. 2005, MNRAS, 357, 1211
Sunyaev, R. A., Markevitch, M., & Pavlinsky, M. 1993, ApJ, 407, 606
Su, M., Slatyer, T. R., & Finkbeiner, D. P. 2010, ApJ, 724, 1044
Supanitsky, A. D. 2014, PhRvD, 89, 023501
Terrier, R., Ponti, G., Bélanger, G., et al. 2010, ApJ, 719, 143
Tsuchiya, K., Enomoto, R., Ksenofontov, L. T., et al. 2004, ApJL, 606, L115
Vasileiou, V., Chiang, J., Omodei, N., et al. 2011, ATel, 3162
Viana, A., & Moulin, E. 2013, in Proc. 33rd Int. Cosmic Ray Conf. 2013, see http://143.107.180.38/indico/contributionDisplay.py?contribId=901&sessionId=3&confId=0
Wang, Q. D., Lu, F. J., Gotthelf, E. V., et al. 2006, MNRAS, 367, 937
Wijnands, R., Zand, J. J. M., Rupen, M., et al. 2006, A&A, 449, 1117
Yang, H.-Y.K., Ruszkowski, M., & Zweibel, E. 2013, MNRAS, 436, 2734
Yoshikoshi, T., Mori, M., Edwards, P. G., et al. 2009, ApJ, 702, 631
Yusef-Zadeh, F., Hewitt, J. W., Wardle, M., et al. 2013, ApJ, 762, 33